Electro-osmotic streaming on application of traveling-wave electric fields

Brian P. Cahill,[1] Laura J. Heyderman,[2] Jens Gobrecht,[2] and Andreas Stemmer[1,*]
[1]*Nanotechnology Group, Swiss Federal Institute of Technology Zurich, CH-8092 Zurich, Switzerland*
[2]*Laboratory for Micro- and Nanotechnology, Paul Scherrer Institute, CH-5232 Villigen PSI, Switzerland*
(Received 16 June 2003; revised manuscript received 7 May 2004; published 14 September 2004)

We describe ac electro-osmotic flow of an aqueous electrolyte on application of a traveling-wave electric field. Depending on the frequency of the applied traveling wave, the interaction of the electric double layer charge and the tangential electric field leads to fluid flow in the direction of the traveling wave. We have derived two theoretical models that describe this flow as a function of the amplitude of the applied electric potential, the signal frequency, and the material properties of the system. The first is based on a capacitative model and is limited to frequencies much lower than the double layer relaxation frequency. The second is an analytical solution of the electrokinetic equations and is also valid at higher frequencies. We provide experimental evidence that streaming takes place on application of a traveling wave of potential by tracing the movements of fluorescent latex beads over a spiral electrode structure. Streaming takes place at applied potentials low enough for the method to be easily integrated into lab-on-a-chip devices.

DOI: 10.1103/PhysRevE.70.036305 PACS number(s): 47.65.+a, 82.70.−y, 66.10.−x, 85.85.+j

I. INTRODUCTION

Lab-on-a-chip systems require controllable pumps capable of pumping small volumes that can be integrated into microsystems. Many of the pumps used in microsystems require the use of moving parts [1]. There is widespread interest in the use of electro-osmotic flow as a noncontact pumping technique using dc electric fields in lab-on-a-chip systems [2–5]. A drawback of dc electro-osmotic flow is that it requires the application of relatively high potentials. Low-potential techniques that can be operated using battery power will enable the integration of electro-osmosis into lab-on-a-chip devices to be optimized, making the systems cheaper and more portable [6,7]. The emergence of microfluidic devices has driven research into electro-osmotic streaming effects over charge-modulated surfaces [8–10,13,11,12] and mixing of fluids flowing over grooved surfaces [14,15].

The arrangement of colloids on application of alternating electric fields has recently been observed [16,17]. Subsequently, experimental studies were made of circulatory flow patterns in aqueous electrolytes over microelectrodes on application of alternating electric fields [12,18–21]. Various models [12,16,21,22] explained this as a form of electro-osmotic flow which became known as alternating current (ac) electro-osmosis. Ajdari suggested using asymmetric electrode structures to drive unidirectional ac electro-osmotic flow [23] and working systems have been implemented [24–27]. Most of these studies have dealt with the frequency-dependent impedance at frequencies much lower than the double layer relaxation frequency and the flow was explained by a combination of equilibrium double layer theory and the Smoluchowski equation [18,21,23,25]. González *et al.* [22] also dealt with the relaxation of the double layer at frequencies of the order of the double layer relaxation frequency by solving the electrokinetic equations using a matched asymptotic expansion method.

Some work has been carried out in the field of electrical engineering to describe electrohydrodynamic pumping of insulating liquids, such as Freon, transformer oil, and corn oil, over traveling-wave electrodes [28–30] on application of ac electric fields at frequencies in the range of the double layer relaxation frequency. Ehrlich and Melcher [28] modeled a type of electro-osmotic streaming in the electric double layer due to traveling-wave excitation for bipolar charge carriers subject to generation and recombination by examining the electrokinetic equations and obtaining both analytical solutions, for certain limiting cases, and a more generally applicable computational solution. They describe a type of streaming caused by the interaction of the electric field with the net charge associated with the electric double layer at a solid-liquid interface as the applied traveling wave approaches the double layer relaxation frequency of the liquid medium.

Another type of electrohydrodynamic pumping at frequencies in the range of the double-layer relaxation frequency has been reported for the case of the interaction of a traveling-wave electric field and an imposed thermal gradient in a fluid. The coupling of this thermal gradient to the temperature dependence of conductivity and dielectric constant leads to local field inhomogeneities that are strong enough to generate deviations from electroneutrality within the bulk of the fluid and leads to convective flow. This phenomenon was first described for insulating fluids [31–33] and later extended to aqueous electrolytes [34–37]. In aqueous electrolytes, the imposed traveling-wave electric field near the electrodes leads to a local temperature rise so that it is no longer necessary to externally impose a thermal gradient. The fluid flow took place in a direction opposite to that of the traveling-wave electric field, although Fuhr *et al.* [35] and Gimsa *et al.* [36] observed another type of fluid flow taking place in the direction of the traveling-wave electric field. No detailed study of this second phenomenon was performed, which both groups explained by means of reference to Ehr-

*FAX: +41 1 632 12 78;
email address: stemmer@nano.mavt.ethz.ch

lich and Melcher [28]. It is likely that the second phenomenon was a form of ac electro-osmosis.

In Sec. II we describe the fabrication of a spiral electrode structure by electron beam lithography with submicron electrode linewidths and gaps and other preparations for the performance of our experiments. In Sec. III we report experimental results of the traveling-wave-induced motion of fluorescent latex beads above the spiral electrode structure. The short wavelength of the traveling-wave electrode structure, 6 μm, enables fluid streaming to take place on applying signals with relatively low amplitudes, below 500 mV. In Sec. IV A we derive the electro-osmotic slip velocity by means of a capacitative model of the equilibrium double layer. This model is limited to frequencies lower than the double layer relaxation frequency. In Sec. IV B we derive a model by solving the electrokinetic equations that is valid for frequencies of the order of the double layer relaxation frequency. This model reduces to the model described in Sec. IV A at lower frequencies. Section IV C describes the conditions at which the linearized theory used in Secs. IV A and IV B is valid. In Sec. IV D we show how both models give the same results at frequencies much lower than the double layer relaxation frequency and relate the experimental results to the second model. A discussion, Sec. V, concludes the paper.

II. MATERIALS AND METHODS

The spiral structures, see Figs. 1(a) and 1(b), were 150 μm in diameter and consisted of four electrodes. The electrode lines were 750 nm wide and separated by 750-nm gaps. The wavelength λ of the traveling wave structure was 6 μm. A spiral configuration was chosen for the convenience of fabricating a traveling-wave electrode structure that does not require complicated interconnections. For ease of bonding, the four connecting lines (40 μm wide and 4 mm long) were placed symmetrically around the spirals with 100-μm-by-200-μm bonding pads at the outer end. The spiral electrode design was exposed in a 150-nm-thick layer of poly(methyl methacrylate) (PMMA) on a silicon substrate coated with a 120-nm layer of silicon dioxide using a LEICA LION LV1 *e*-beam writer. This machine is equipped with continuous path control that allows structuring of large areas without stitching errors. Lines of various widths can be added using a defocused exposure [38]. The exposed areas were then transferred into metal using the following lift-off procedure; a 10-nm titanium/70-nm aluminum layer was deposited by evaporation. The thin layer of titanium provided good adhesion of the aluminum to the silicon substrate. Unwanted aluminum deposited on the PMMA was removed in acetone using ultrasonic agitation. The structures were coated with a 50-nm-thick protective insulating layer of hexafluoropropene (HFP), a Teflon-like fluorocarbon, by plasma-enhanced chemical vapor deposition [39]. Bonding wires were used to connect each of the four electrodes to a printed circuit board. The printed circuit board was connected by means of coaxial cables to a four-phase voltage supply.

A purpose-built four-phase voltage supply was developed to generate square-wave-form traveling-wave signals in the range between 10 kHz and 5 MHz. Four-phase square-wave traveling-wave signals were applied to the four electrodes so that there was a 90° phase difference between the signals applied to each electrode. Figure 1(c) shows the form of these square waves. Developing a square-wave signal generator requires much less expense than developing a four-phase sine-wave signal generator and also has the advantage of operating across a relatively wide bandwidth. The amplitude of the applied signal was measured using a Kikusui COR5521U 40-MHz digital oscilloscope.

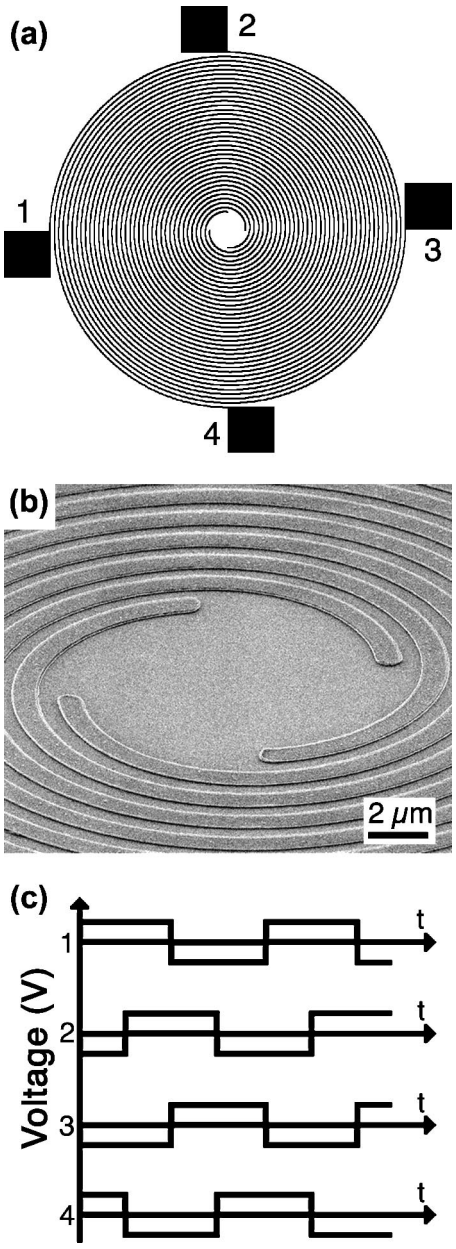

FIG. 1. (a) Schematic drawing of the spiral electrode structure, four electrodes are arranged in a spiral structure and numbered 1–4. (b) Scanning electron microscope image of the center of the spiral electrode structure. (c) Square-wave traveling-wave signals 1–4 that are applied to electrodes 1–4 as shown in (a).

Three KCl solutions in the concentration range between 2×10^{-4} and 10^{-3} M were prepared and the conductivity of each was measured to be 2.00, 4.19 and 8.36 mS/m respectively, using a Knick 911 Conductivity Meter with a ZU 6985 four-electrode cell (Knick GmbH, Berlin, Germany). 200-nm-diameter Fluoresbrite carboxylate latex beads (Polysciences, Warrington, PA, USA) with yellow green fluorescence were suspended in the aqueous KCl solutions at a concentration of 0.0013% v/v.

A microscope cover slip was placed over the spiral using double-sided-adhesive tape of 100-μm thickness as a spacer. After introducing the latex bead suspension into this cavity, bead movement was observed and images acquired by fluorescent light microscopy using a Nikon Eclipse 800 microscope and a Cohu charge-coupled device (CCD) camera. Digital movies of the latex bead movement were made after focusing a 40× objective with 0.75 numerical aperture onto the electrode surface, thus only beads within the depth of field, less than 1 μm, could be observed. The spatial extent of the recorded frames stretched laterally from one side of the spiral to the other but the vertical extent was restricted in order to allow a higher frame rate to be recorded. Measurements of the velocity of several beads were made for each frequency and excitation potential, and the average velocity and standard deviation were calculated. The velocity was estimated by measuring the distance traveled by a bead as tracked from the digital movie and dividing by the time separating these digital movie frames.

III. EXPERIMENTAL RESULTS

Movement of fluorescent latex beads was observed on application of a traveling wave of potential to the spiral electrode structure at frequencies of the order of the double layer relaxation frequency of the prepared electrolytic solutions. On applying a traveling-wave signal in the direction of the center of the spiral, the beads moved towards the center of the spiral. On reversing the direction of travel of the traveling-wave signal, the beads reversed direction and moved from the center towards the edge of the spiral. Thus it is clear that the traveling wave of potential was responsible for the movement of the latex beads. Motion of the beads was observed within a couple of microns of the surface of the chip.

Experiments were carried out to evaluate the dependence of the velocity of the fluorescent latex beads on the signal frequency and applied potential. The velocity was measured for various signal frequencies at different applied potentials for each of the three electrolytic solutions. Figure 2 shows three graphs, one for each of the three electrolytic solutions, that respectively show three curves for the velocity plotted against frequency at different applied potentials.

The general behavior consistently shows that at low and high frequencies the velocity tends to zero while the peak velocity occurs at a frequency that is a little less than half the double layer relaxation frequency. The double layer relaxation time τ is related to the time required for the electric double layer to respond to a dynamic electric field and is given by $\tau=\varepsilon_2/\sigma$, where ε_2 is the dielectric constant of the

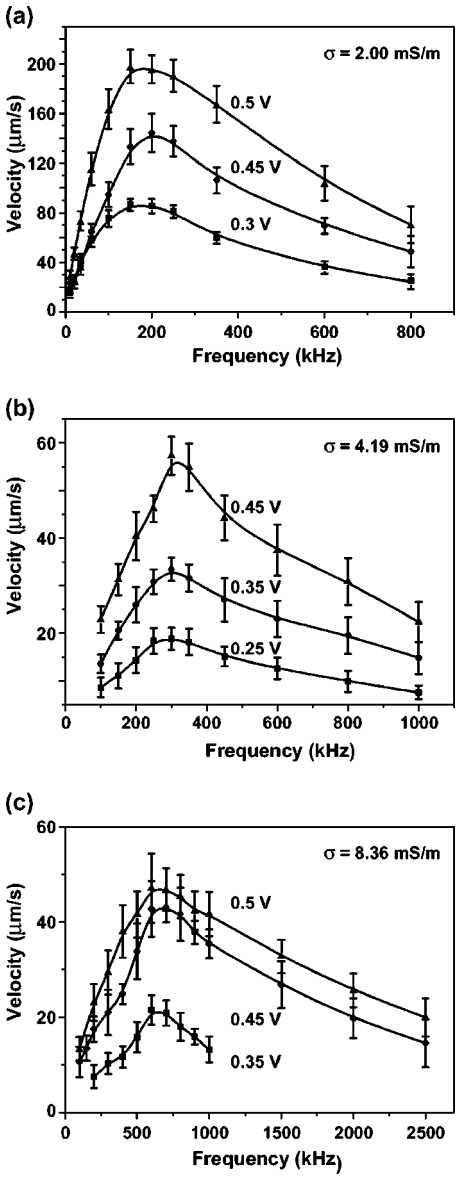

FIG. 2. Experimentally measured values of the velocity of the fluorescent latex beads plotted against frequency at different applied potentials, as denoted on each graph. Figures (a), (b), and (c) present results obtained using aqueous electrolytes with the respective medium conductivities: 2.00, 4.19, and 8.36 mS/m. The fitted curves are to aid the eye.

electrolyte and σ is the electrolyte conductivity. The lower conductivity electrolytes have higher velocities and the frequency of maximum velocity is lower for the same applied potential. For each electrolytic solution, the frequency of maximum velocity appears to be independent of the applied potential.

Measurement of the dependence of the velocity of the fluorescent latex beads on applied potential was made by first ascertaining the frequency of the peak velocity and then making a set of movies at this frequency for various applied potentials. Figure 3 shows the dependence of the velocity on applied potential for a solution with conductivity of 4.19 mS/m at 300 kHz. The velocity is plotted against the square of the potential applied to the electrodes and fitted to

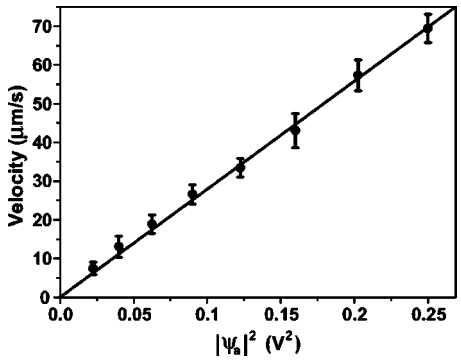

FIG. 3. Experimentally measured values of the velocity of the fluorescent latex beads plotted against the square of applied potential with a medium conductivity of 4.19 mS/m ($1/\kappa = 18.1$ nm) and at an applied frequency of 300 kHz. A linear fit was applied showing the proportionality of velocity to the square of the applied potential, $|\psi_a|^2$.

a straight line through the origin. Figure 3 shows clearly that the velocity is directly proportional to the square of the applied potential. On increasing the applied potential above 500 mV, the latex beads were attracted to the electrode structure by positive dielectrophoresis [40] so that it was not possible to study streaming at higher potentials.

IV. THEORETICAL MODELS

Electro-osmosis is an electrokinetic phenomenon, in which ions in solution migrate in the presence of an electric field, causing a body force on the liquid that results in fluid flow. Net flow requires charge separation; that is, that the local net charge density is nonzero. The formation of the electric double layer results in such charge separation at a charged interface and applying an electric field in a direction tangential to the interface causes electro-osmotic flow [41–43].

Figure 4 shows a simplified explanation of how traveling waves cause directed electro-osmotic flow for a traveling wave traveling from left to right. The magnitude of electro-osmotic flow is determined by the interaction of the electric double layer charge with the electric field, more specifically, the electric field tangential to the interface. In the case of these models, the magnitude and phase of these two quantities is dependent on the frequency of the applied traveling wave. The frequency-dependent phase difference between the signal applied to the electrodes and the resultant electric field in the electrolyte is more complex than shown here but to understand the phenomenon it is more important to note the phase difference between the electric double layer and the tangential electric field. Figure 4(a) shows the situation at very low frequencies, the double layer charge and tangential electric field are 90° out of phase and no directed flow can take place. Also the tangential component of the electric field is attenuated considerably by the formation of the double layer. As the frequency of the applied traveling wave electric field approaches a certain characteristic frequency ω_c, as shown in Fig. 4(b), the phase difference between the electric double layer and the tangential electric field decreases so that

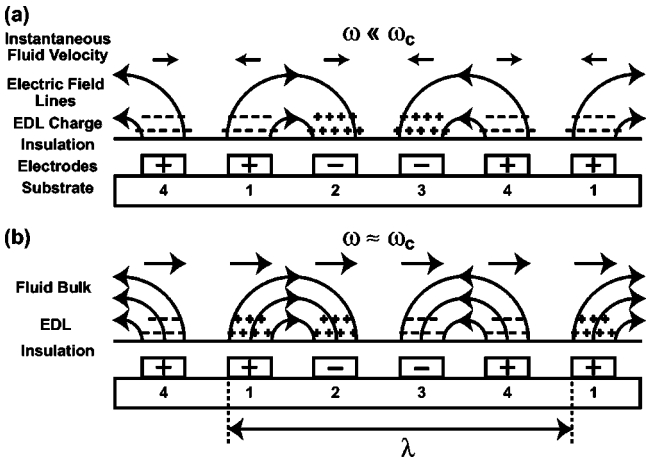

FIG. 4. Diagram explaining the mechanism of electro-osmotic flow due to the application of a traveling wave that travels from left to right. A plus / minus sign on an electrode signifies that a positive / negative potential is instantaneously applied to the electrode. A plus /minus sign above the insulating layer signifies that the electric double layer (EDL) has a surplus of positive / negative ions. These illustrations show uniform field lines although the field lines will be quite nonuniform in practice. The density of the field lines indicates the strength of the field. (a) No time-averaged electro-osmotic flow takes place at frequencies much lower than the characteristic frequency ω_c. (b) At frequencies of the order of ω_c, the interaction between the surface charge density associated with the electric double layer and the tangential electric field causes nonzero time-averaged fluid flow.

a time-averaged flow in the same direction as the traveling wave takes place, the tangential electric field increases in strength and the electric double layer charge density may decrease. The tangential component of the electric field over electrodes 1 and 2 points towards the right-hand side and the positive ions surrounding these electrodes migrate from left to right. Analogously, the tangential component of the electric field over electrodes 3 and 4 points towards the left-hand side and the negative ions surrounding these electrodes also migrate from left to right. Hence a time-averaged flow takes place in the same direction over all electrodes with a velocity that depends on the phase difference between the tangential electric field and the double layer charge density as well as the absolute value of these two quantities. The directionality of the flow may be controlled externally by changing the direction of travel of the traveling-wave electric field.

The potential distribution is determined by capacitances of the system: (i) the insulating layer capacitance, (ii) the Stern layer capacitance, and (iii) the capacitance of the electric double layer. We choose to neglect the Stern layer capacitance but it could be easily included. We will show how the capacitance of an insulating layer affects the frequency at which electro-osmotic takes place.

Figure 5 shows the important interfaces for our model. The interface between the substrate and the insulation layer, denoted by *a*, is in the plane of the electrode structure that provides electrical excitation to our system. The interface between the insulation layer and the electrolyte is denoted by *b*. The *c* plane is where the electric double layer can be

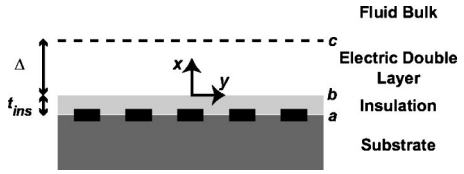

FIG. 5. The *a* plane is the plane between the insulating layer and the substrate where the electroodes are located. The *b* plane is the plane between the insulating layer and the fluid. The *c* plane is where the electric double layer can be considered to end and the fluid bulk begins. The x/y directions are defined as normal /tangential to the interface, respectively. The dashed line shows the extent of the electric double layer. The origin is in the *b* plane so that $x=0$ at the interface between the insulating layer and the electrolyte. Δ is a distance normal to the surface of the dielectric layer at which the charge separation due to the electric double layer becomes negligible. t_{ins} is the thickness of the insulating layer.

considered to end and the fluid bulk begins, that is, where the volume charge density is zero and the field in the fluid obeys the Laplace equation. The subscripts *a*, *b*, and *c* will be used throughout the paper to denote a variable evaluated in the *a*, *b*, and *c* planes, respectively. The *x* and *y* directions are, respectively, normal and parallel to these planes. We choose *x* to be zero in the *b* plane. The insulation of the electrodes serves to prevent Faradaic current, although, this analysis would also be applicable to perfectly polarizable electrodes.

We presume that the electrical potential at the dielectric interface and throughout the electrolyte takes the form of a sinusoidal wave traveling in the *y* direction:

$$\psi(x,y,t) = \mathrm{Re}\{\hat{\psi}(x)\exp[i(\omega t - k_y y)]\}, \tag{1}$$

where $\hat{\psi}$ is the complex amplitude of the potential, *i* denotes $\sqrt{-1}$, ω is the angular frequency of the applied traveling wave of potential, *t* is time, and k_y is the propagation constant of the traveling wave, that is, $k_y = 2\pi/\lambda$, where λ is the wavelength of the traveling wave as shown in Fig. 4(b). The diacritical mark "^" signifies a complex quantity. We assume that the first harmonic of the Fourier series describing the square wave predominates.

The double layer relaxation frequency is the frequency for which $\omega\tau=1$. It will prove useful to state the approximate width of the electric double layer, the inverse Debye length, in terms of the diffusion coefficient *D* and τ :

$$\kappa^2 \approx \frac{1}{\tau D}. \tag{2}$$

A. Low-frequency model

We will first derive an expression for the electro-osmotic slip velocity in a fashion similar to Ajdari [23]. The following assumptions are made: (i) the frequency is much lower than the double layer relaxation frequency, $\omega\tau \ll 1$ so that the electric double layer is fully equilibrated, (ii) the Debye length is much smaller than the electrode dimensions, $k_y \ll \kappa$, as we shall presume throughout this paper and as applies to our experimental conditions, and (iii) the wavelength of the electrode structure is much longer than the insulating layer thickness, $k_y t_{ins} \ll 1$, so the insulating layer can be viewed as "thin" allowing it to be approximated as a capacitor in series with the double layer.

The system can be described by two capacitors in series, the capacitance per unit area of the insulating layer $C_{ins} = \varepsilon_1/t_{ins}$ and the capacitance per unit area of the electric double layer $C_{edl} = \varepsilon_2\kappa$. This presumes that the potential drop across the double layer is less than kT/ze, so that we can presume a linear relationship between the capacitance of the double layer and the inverse Debye length κ, where *z* is the ion valence, *e* is the electron charge, *k* is Boltzmann's constant, *T* is the absolute temperature. The sum of these capacitances is given by $C_{sum} = \varepsilon_2\kappa/(1+\delta)$ where $\delta = t_{ins}\varepsilon_2\kappa/\varepsilon_1$.

Ohm's law describes ion transport in the bulk solution. Thus in the *c* plane, Ohm's law applied in the direction normal to the surface gives

$$\mathbf{n}\cdot\boldsymbol{J} = -\sigma \left.\frac{\partial \psi}{\partial x}\right|_c = C_{sum}\frac{\partial(\psi_a - \psi_c)}{\partial t}, \tag{3}$$

where **n** is a unit vector normal to the surface.

The potential in the bulk fluid and in the *c* plane obeys the Laplace equation, $\nabla^2\psi = 0$, so that from the form of the traveling wave and if the potential decays to zero very far away from the surface, it can be shown that $\partial\psi/\partial x|_c = -k_y\psi_c$. By separation of variables it can be shown that

$$\hat{\psi}_c = \frac{\hat{\psi}_a}{1 - i(\omega_c/\omega)}, \tag{4}$$

where the characteristic frequency ω_c is given by

$$\omega_c = \frac{\sigma k_y}{C_{sum}} = \frac{k_y(1+\delta)}{\kappa\tau}. \tag{5}$$

The Smoluchowski equation [44] forms the basis of much work in electrokinetics and describes how the formation of the electric double layer gives rise to a surface charge density σ_D, which interacts with the tangential electric field E_t to cause an electro-osmotic flow with slip velocity v_{slip}:

$$v_{slip} = \frac{\sigma_D E_t}{\kappa\eta}, \tag{6}$$

where the surface charge density is given by

$$\sigma_d = C_{sum}(\psi_c - \psi_a) \tag{7}$$

and the tangential electric field follows from the definition of the traveling wave,

$$E_t = \mathrm{Re}\{ik_y\hat{\psi}_c(x)\exp[i(\omega t - k_y y)]\}. \tag{8}$$

The Smoluchowski equation is valid if the potential drop across the double layer is less than kT/ze.

The time average of the product of two complex quantities is equal to half of the product of one of the quantities and the complex conjugate of the other. The time-averaged slip velocity $\langle v_{slip}\rangle$ is given by

$$\langle v_{slip} \rangle = \frac{\varepsilon_2 |\hat{\psi}_a|^2 \omega\tau}{2\eta\kappa \left| \frac{1}{\kappa} + \frac{i\omega\tau}{k_y} + \frac{t_{ins}\varepsilon_2}{\varepsilon_1} \right|^2}. \quad (9)$$

For Eq. (9) to be valid ω_c must be much less than the double layer relaxation frequency. Otherwise the assumptions of the model are not fulfilled because the double layer is no longer in quasiequilibrium. The characteristic frequency ω_c is the same as in Ajdari's model [23]. In principle, the ac electro-osmotic phenomenon is identical to that described by Ajdari, we describe a traveling wave here and Ajdari described a standing wave.

B. High-frequency model

We have chosen to develop a model that will be able to describe the effect of double layer relaxation on ac electro-osmotic flow because for input data pertaining to our experiment ω_c is greater than the double layer relaxation frequency because of our use of a insulation layer and the relatively short wavelength of the electrode structure (6 μm). Although the insulation layer thickness (50 nm) is not much greater than the Debye length (12.8–26.3 nm), the dielectric constant is 40 times smaller than that of water so that δ is much greater than 1 (80–120) so that ω_c exceeds the double layer relaxation frequency.

1. Basic model and governing equations

The electrokinetic equations are a set of partial differential equations that relate electrical potential, ion densities, and fluid velocities in an electrolyte [22,28,41,45,46]. We shall presume that the fluid viscosity, dielectric constant, and diffusion coefficient take the same value in the electric double layer as in the bulk fluid. We presume that the dielectric surface is intrinsically uncharged so that the formation of the electric double layer is a direct result of applying the traveling-wave signal. We shall limit our analysis to low potentials, as we shall discuss in more detail below. The variation of ion density and potential in a conducting fluid at a dielectric interface on application of low amplitude ac potentials has previously been dealt with in the literature [47,48].

The ion conservation equation relates the rate of change of the number of ions per unit volume to the net rate at which ions enter that volume:

$$\frac{\partial n_j}{\partial t} = -\nabla \cdot \mathbf{f}_j, \quad (10)$$

where n_j is the number of ions of type j per unit volume, and $\mathbf{f}_j$ is the flux density. The flux density describes the number of ions that pass through a surface of a volume element per second and consists of terms related to diffusion, conduction and convection, respectively:

$$\mathbf{f}_j = -D_j \left(\nabla n_j + \frac{z_j e n_j}{kT} \nabla \psi \right) + n_j \mathbf{v}, \quad (11)$$

where D_j is the diffusion coefficient of ions of type j, z_j is the valence of ions of type j, $\boldsymbol{v}$ is the fluid velocity. The electric Reynolds number R_{el} [49] is the ratio of the characteristic times for electric double layer relaxation τ and for ion transport due to convection $1/(k_y v_y)$:

$$R_{el} = k_y v_y \tau, \quad (12)$$

where v_y is the fluid velocity in the y direction. For the fluid velocity observed experimentally and the double layer relaxation times corresponding to the electrolytic solutions used in our experiments, the electric Reynolds number is much less than 1. Hence the double layer forms much more quickly than the convection can transport ions between neighboring electrodes, allowing us to neglect the charge convection term $n_j \boldsymbol{v}$ from Eq. (11).

Poisson's equation relates electrical potential to the local charge density in the region of the electric double layer:

$$\nabla^2 \psi = -\sum_{j=1}^{N} \frac{z_j e n_j}{\varepsilon_2}, \quad (13)$$

where N is the number of ion types present in the electrolyte. If the local charge density is zero, Poisson's equation reduces to Laplace's equation:

$$\nabla^2 \psi = 0. \quad (14)$$

For an incompressible fluid of uniform mass density and viscosity, fluid flow is governed by the incompressible Navier-Stokes equations:

$$\nabla \cdot \mathbf{v} = 0 \quad \text{and} \quad (15)$$

$$\rho_f \frac{\partial \mathbf{v}}{\partial t} = \eta \nabla^2 \mathbf{v} - \nabla p - \sum_{j=1}^{N} z_j e n_j \nabla \psi, \quad (16)$$

where ρ_f is the fluid density, η is the fluid viscosity, and p is the pressure. If the Reynolds number of the flow is much less than 1, the inertial term of Eq. (16) may be considered negligible.

The analysis of electro-osmosis combined with nonuniform surface charge has previously been examined for colloids [50] and for planar surfaces [3,8,9,11,12,51]. If the surface charge varies over a distance that is much greater than the double layer, it is usual to decouple the problem into two problems: (i) inside the double layer the pressure gradient can be considered negligible so that the electro-osmotic slip velocity is given by the Smoluchowski equation and (ii) outside the double layer the charge density is negligible so that the fluid dynamic problem can be solved using the electro-osmotic slip velocity as a boundary condition [52]. Our case is slightly different to these cases because the surface potential is a function of time and position at frequencies of the order of the double layer relaxation frequency. We choose to deal with this problem by following the example of Anderson [50] and considering flow in the direction normal to the surface inside the double layer to be negligible so that the vector components of Eq. (16) reduce to

$$\frac{\partial^2 v_y}{\partial x^2} = \frac{\partial p}{\partial y} - \varepsilon_2 \nabla^2 \psi \frac{\partial \psi}{\partial y} \quad \text{and} \quad (17)$$

$$\frac{\partial p}{\partial x} = \varepsilon_2 \nabla^2 \psi \frac{\partial \psi}{\partial x} = \varepsilon_2 \left(\frac{\partial^2 \psi}{\partial x^2} - k_y^2 \psi \right) \frac{\partial \psi}{\partial x}. \tag{18}$$

Equation (18) can be integrated directly to obtain an expression for the pressure that can be used to state $\partial p/\partial y$ as

$$\frac{\partial p}{\partial y} = \varepsilon_2 \frac{\partial \psi}{\partial x} \frac{\partial^2 \psi}{\partial x \partial y} - \varepsilon_2 k_y^2 \psi \frac{\partial \psi}{\partial y}. \tag{19}$$

2. Frequency-dependent ionic concentration in the electric double layer

In order to describe the local ion density, we choose to split it into two components, the ion density in the bulk fluid n_j^∞ and a small sinusoidal disturbance δn_j:

$$n_j(x,y,t) = n_j^\infty + \delta n_j(x,y,t), \tag{20}$$

where δn_j takes the form of the applied traveling wave, $\delta n_j = \mathrm{Re}\{\delta \hat{n}_j(x) \exp[i(\omega t - k_y y)]\}$, $\delta \hat{n}_j$ is the complex amplitude of δn_j, and $\delta n_j < n_j^\infty$. From Eqs. (10), (11), and (20), we obtain the following:

$$\frac{\partial \delta n_j}{\partial t} = D_j \left(\nabla^2 \delta n_j + \frac{z_j e}{kT} [(n_j^\infty + \delta n_j) \nabla^2 \psi + \nabla \delta n_j \cdot \nabla \psi] \right). \tag{21}$$

Considering an electrolyte, with ion densities, n_1 and n_2, and valences, z_1 and z_2, where the subscripts 1 and 2 represent cations and anions, respectively, we obtain the following simultaneous equations:

$$\mathrm{Re}\{i\omega \delta \hat{n}_1 \exp[i(\omega t - k_y y)]\} = D_1 \left(\nabla^2 \delta n_1 + \frac{z_1 e}{kT} [(n_1^\infty + \delta n_1) \nabla^2 \psi + \nabla \delta n_1 \cdot \nabla \psi] \right) \quad \text{and} \tag{22}$$

$$\mathrm{Re}\{i\omega \delta \hat{n}_2 \exp[i(\omega t - k_y y)]\} = D_2 \left(\nabla^2 \delta n_2 + \frac{z_2 e}{kT} [(n_2^\infty + \delta n_2) \nabla^2 \psi + \nabla \delta n_2 \cdot \nabla \psi] \right). \tag{23}$$

By restricting ourselves to strong symmetrical electrolytes, we may relate the properties of ions of type 2 to those of ions of type 1. The diffusion coefficient of each type of ion is identical, $D = D_1 = D_2$, this can be considered true for KCl. The bulk concentration of both ions is the same: $n^\infty = n_2^\infty = n_1^\infty$. The anions and cations possess charge of equal magnitude and opposite polarity, so that the valence is also opposite and equal: $z_1 = -z_2$. By introducing the following two substitutions:

$$g = \frac{\delta n_1 - \delta n_2}{2} = \mathrm{Re}\{\hat{g}(x) \exp[i(\omega t - k_y y)]\} \quad \text{and} \tag{24}$$

$$h = \frac{\delta n_1 + \delta n_2}{2} = \mathrm{Re}\{\hat{h}(x) \exp[i(\omega t - k_y y)]\}, \tag{25}$$

and by subtracting Eq. (23) from Eq. (22), we reduce these simultaneous equations to one differential equation:

$$\mathrm{Re}\{i\omega \hat{g} \exp[i(\omega t - k_y y)]\} = D \left(\nabla^2 g + \frac{z_1 e}{kT} [(n^\infty + h) \nabla^2 \psi + \nabla h \cdot \nabla \psi] \right). \tag{26}$$

At low applied potentials, δn_1 and δn_2 have equal amplitudes and are 180° out of phase with each other, this requires that $g < n^\infty$, which restricts us to applying low potential as we shall discuss later. It also means that h may be considered negligible throughout the electrical double layer and the bulk fluid. In addition, by inserting Poisson's equation, Eq. (13), into Eq. (26) it can be shown that

$$i\omega \hat{g} = D(\nabla^2 \hat{g} - \kappa^2 \hat{g}), \tag{27}$$

where the inverse Debye length κ [53,54] is described by

$$\kappa^2 = \frac{2 z^2 e^2 n^\infty}{\varepsilon_2 kT}. \tag{28}$$

Separation of variables further simplifies Eq. (27):

$$\kappa^2 (1 + i\omega\tau) \hat{g} = \nabla^2 \hat{g} = \left(\frac{\partial^2 \hat{g}}{\partial x^2} - k_y^2 \hat{g} \right), \tag{29}$$

where the second term on the right-hand side is the second derivative of g with respect to y. Further separation of variables gives

$$\hat{g} = \frac{1}{\kappa^2 \left(1 + \frac{k_y^2}{\kappa^2} + i\omega\tau \right)} \frac{\partial^2 \hat{g}}{\partial x^2}. \tag{30}$$

If $k_y \ll \kappa$, then the following simplification is valid:

$$\hat{g} \approx \frac{1}{\kappa^2 (1 + i\omega\tau)} \frac{\partial^2 \hat{g}}{\partial x^2}. \tag{31}$$

The following boundary conditions can be used to solve the differential equation given by Eq. (31):

$$g|_{x \to \infty} = 0, \tag{32}$$

$$\left. \frac{\partial g}{\partial x} \right|_{x \to \infty} = 0, \text{ and} \tag{33}$$

$$\left. \frac{\partial g}{\partial x} \right|_b = \mathrm{Re} \left\{ - \frac{z_1 e n^\infty}{kT} \left. \frac{\partial \hat{\psi}}{\partial x} \right|_b \exp[i(\omega t - k_y y)] \right\}. \tag{34}$$

Equations (32) and (33) follow from the electroneutrality of the bulk solution. Equation (34) follows from the imperviousness of the dielectric surface to ions and results from applying the following to Eq. (11):

$$\mathbf{n} \cdot \boldsymbol{f}_j|_b = 0. \tag{35}$$

Using the boundary conditions given by Eqs. (32)–(34), the solution to Eq. (31) is

$$\hat{g} = \frac{z_1 e n^\infty \exp(-\kappa x \sqrt{1 + i\omega\tau})}{kT \kappa \sqrt{1 + i\omega\tau}} \left. \frac{\partial \hat{\psi}}{\partial x} \right|_b. \tag{36}$$

3. Frequency-dependent potential distribution in the electrolyte

It will prove useful to state g in terms of ψ_b by finding a relation between ψ_b and $\partial\hat{\psi}/\partial x|_b$. We can do this by examining Poisson's equation, Eq. (13):

$$\nabla^2\psi = \frac{\partial^2\psi}{\partial x^2} + \frac{\partial^2\psi}{\partial y^2} = -\frac{2z_1 e}{\varepsilon} g. \tag{37}$$

As the frequency increases, Eq. (37) reduces to Laplace's equation, Eq. (14). Melcher [55] describes a method to solve frequency-dependent equations of this sort that are required to simultaneously satisfy both Poisson's and Laplace's equations, by considering the potential to be the sum of a particular solution, φ, that satisfies Poisson's equation and a homogeneous solution, ϕ, that satisfies Laplace's equation:

$$\psi(x,y,t) = \varphi(x,y,t) + \phi(x,y,t). \tag{38}$$

By solving Laplace's equation with the boundary condition that $\hat{\phi}_b$ is the complex amplitude of the potential in the b plane and the potential decays to zero at infinity, ϕ can be shown to be of the form

$$\phi(x,y,t) = \mathrm{Re}\{\hat{\phi}_b \exp[i(\omega t - k_y y) - k_y x]\}. \tag{39}$$

It is a reasonable assumption that the exponential decay of φ takes the same form as the exponential decay of g so that φ is given by Eq. (36):

$$\varphi(x,y,t) = \mathrm{Re}\{\hat{\varphi}_b \exp[i(\omega t - k_y y) - \kappa x\sqrt{1+i\omega\tau}]\}, \tag{40}$$

where $\hat{\varphi}_b$ is the complex amplitude of φ in the b plane.

Using Eqs. (36)–(40) it is elementary to state $\hat{\psi}$ in terms of $\hat{\psi}_b$:

$$\hat{\psi} = \hat{\psi}_b \frac{\dfrac{\exp(-\kappa x\sqrt{1+i\omega\tau})}{\kappa\sqrt{1+i\omega\tau}} + \dfrac{i\omega\tau\exp(-k_y x)}{k_y}}{\dfrac{1}{\kappa\sqrt{1+i\omega\tau}} + \dfrac{i\omega\tau}{k_y}}, \tag{41}$$

and $\partial\hat{\psi}/\partial x|_b$ in terms of $\hat{\psi}_b$,

$$\left.\frac{\partial\hat{\psi}}{\partial x}\right|_b = -\hat{\psi}_b \frac{1+i\omega\tau}{\dfrac{1}{\kappa\sqrt{1+i\omega\tau}} + \dfrac{i\omega\tau}{k_y}}. \tag{42}$$

Also, $\hat{g}$ takes the form

$$\hat{g} = -\frac{n^\infty \hat{\psi}_b}{\kappa}\frac{z_1 e}{kT}\frac{\sqrt{1+i\omega\tau}\exp(-\kappa x\sqrt{1+i\omega\tau})}{\dfrac{1}{\kappa\sqrt{1+i\omega\tau}} + \dfrac{i\omega\tau}{k_y}}. \tag{43}$$

4. Boundary condition between insulating layer and electrolyte

We can relate $\hat{\psi}_b$ to the potential applied to the electrodes, $\hat{\psi}_a$, by considering the boundary conditions at the interface between the insulating layer and the electrolyte. From Gauss's law it can be shown that the **D** field above and below the interface, denoted by $\mathbf{D}_+$ and $\mathbf{D}_-$, respectively, are equal if there are no real charges on the interface [47,48]:

$$0 = \mathbf{n}\cdot(\mathbf{D}_- - \mathbf{D}_+) = \mathbf{n}\cdot(\varepsilon_1\mathbf{E}_- - \varepsilon_2\mathbf{E}_+), \tag{44}$$

where ε_1 is the dielectric constant of the insulating layer and $\mathbf{E} = -\boldsymbol{\nabla}\psi$. If $k_y t_{ins} \ll 1$, where t_{ins} is the thickness of the insulating layer, then the component of the electric field in the x direction is constant throughout the insulating layer and is equal to the potential difference across the layer divided by t_{ins}. From Eq. (42) and the continuity of ψ_b across the interface, Eq. (44) reduces to

$$\frac{\varepsilon_2(1+i\omega\tau)\hat{\psi}_b}{\dfrac{1}{\kappa\sqrt{1+i\omega\tau}} + \dfrac{i\omega\tau}{k_y}} = \frac{\varepsilon_1(\hat{\psi}_a - \hat{\psi}_b)}{t_{ins}}. \tag{45}$$

By separation of variables, we can relate $\hat{\psi}_b$ to $\hat{\psi}_a$:

$$\hat{\psi}_b = \hat{\psi}_a \frac{\dfrac{1}{\kappa\sqrt{1+i\omega\tau}} + \dfrac{i\omega\tau}{k_y}}{\dfrac{1}{\kappa\sqrt{1+i\omega\tau}} + \dfrac{i\omega\tau}{k_y} + \dfrac{t_{ins}\varepsilon_2}{\varepsilon_1}(1+i\omega\tau)}. \tag{46}$$

This enables us to restate Eqs. (41) and (43) in terms of $\hat{\psi}_a$:

$$\hat{\psi} = \hat{\psi}_a \frac{\dfrac{\exp(-\kappa x\sqrt{1+i\omega\tau})}{\kappa\sqrt{1+i\omega\tau}} + \dfrac{i\omega\tau\exp(-k_y x)}{k_y}}{\dfrac{1}{\kappa\sqrt{1+i\omega\tau}} + \dfrac{i\omega\tau}{k_y} + \dfrac{t_{ins}\varepsilon_2}{\varepsilon_1}(1+i\omega\tau)} \quad \text{and} \tag{47}$$

$$\hat{g} = -\hat{\psi}_a \frac{\dfrac{n^\infty}{\kappa}\dfrac{z_1 e}{kT}\sqrt{1+i\omega\tau}\exp(-\kappa x\sqrt{1+i\omega\tau})}{\dfrac{1}{\kappa\sqrt{1+i\omega\tau}} + \dfrac{i\omega\tau}{k_y} + \dfrac{t_{ins}\varepsilon_2}{\varepsilon_1}(1+i\omega\tau)}. \tag{48}$$

For this analysis to be valid the following condition must be fulfilled: $g < n^\infty$. As g approaches values close to n^∞, this model can no longer be considered valid, as the assumptions inherent in our model will lead to error. At high electrical potentials, this analytical solution is invalid, as the concentration of ions in the electric double layer will be disturbed in a more complicated manner than discussed here.

5. Electro-osmotic slip velocity

We can evaluate the slip velocity by integrating Eq. (17) twice with respect to x. The boundary conditions for this integral are the no slip boundary condition, that the fluid velocity at the dielectric surface is constrained to be zero,

and that the fluid velocity at a distance many times the Debye length from the dielectric surface reaches a constant slip velocity v_{slip}, so that v_{slip} is given by

$$v_{slip} = \frac{2z_1 e}{\eta} \int_0^{\Delta} \int_x^{\Delta} \left(\frac{\partial p}{\partial y} - g \frac{\partial \psi}{\partial y} \right) dx dx, \tag{49}$$

where Δ is a distance normal to the dielectric interface at which the charge separation due to the electric double layer becomes negligible and at which the fluid velocity is v_{slip}. Thus by inserting the first derivative of Eq. (1) with regard to y and Eqs. (47) and (48) into Eq. (49) and allowing Δ to approach infinity (so that we include all the charge contained in the electric double layer) and performing the double integration we can show that the time-averaged slip velocity $\langle v_{slip} \rangle$ is given by

$$\langle v_{slip} \rangle = \frac{\frac{\varepsilon_2 |\hat{\psi}_a|^2 \omega\tau}{2\eta\kappa} \frac{1}{\mathrm{Re}\{\sqrt{1+i\omega\tau}\}}}{\left| \frac{1}{\kappa\sqrt{1+i\omega\tau}} + \frac{i\omega\tau}{k_y} + \frac{t_{ins}\varepsilon_2}{\varepsilon_1}(1+i\omega\tau) \right|^2}, \tag{50}$$

where a complex quantity surrounded by straight brackets denotes the absolute value of the complex quantity and we have neglected some terms that are insignificant because $k_y \ll \kappa$ and the time average of $\partial p/\partial y$ is zero. For traveling wave potentials, the time average of Eq. (19) is zero and it does not affect the time-averaged electro-osmotic slip velocity.

Equation (50) can be shown to be compatible with an equation derived for similar conditions by Ehrlich and Melcher [28] by replacing $\hat{\psi}_a$ with $\partial\hat{\psi}/\partial x|_b$ by means of Eqs. (42) and (46). Equation (50) has the advantage that the slip velocity can be related much more easily to experimental results because it is more practical to hold the excitation voltage applied to the electrodes constant. This equation shows that the slip velocity tends to zero at frequencies much higher or lower than the double layer relaxation frequency as was shown by our experiments. The frequency dependence of slip velocity is more complicated than that derived by Ehrlich and Melcher [28], being dependent on the Debye length, propagation constant, thickness of the insulating layer, and the dielectric constant of the insulating layer and fluid, in addition to the relaxation time and frequency. The electro-osmotic slip velocity is proportional to the square of the excitation potential as shown experimentally in Fig. 3. The slip velocity is proportional to the Debye length, this means the slip velocity is inversely proportional to the square root of the concentration of the electrolyte.

In Fig. 6, three graphs are plotted that show how this type of streaming can be optimized. Figure 6(a) shows how the frequency of maximum slip velocity shifts to higher frequencies as the wavelength of the traveling-wave electrode array decreases. Figure 6(b) shows how the frequency of maximum slip velocity shifts very slightly to lower frequencies as the factor $t_{ins}\varepsilon_2/\varepsilon_1$ decreases. These graphs show that the miniaturization of the dimensions of the setup is the most important factor enabling this form of electro-osmotic flow to take place over the traveling-wave spiral. The slip velocity increases as dimensions associated with the experimental setup, the wavelength of the traveling-wave electrode structure, and the thickness of the insulating layer, decrease. If the dimensions are too large, the streaming will be of too low velocity for the force on the latex beads to overcome Brownian motion, at least within the terms of validity of our model. The term relating to the thickness of the insulating layer is coupled to the ratio of the dielectric constant of the medium to that of the insulating layer itself. Thus thin layers of high dielectric constant material are the best material choice to optimize this type of electro-osmotic transport if it is necessary to use an insulating layer.

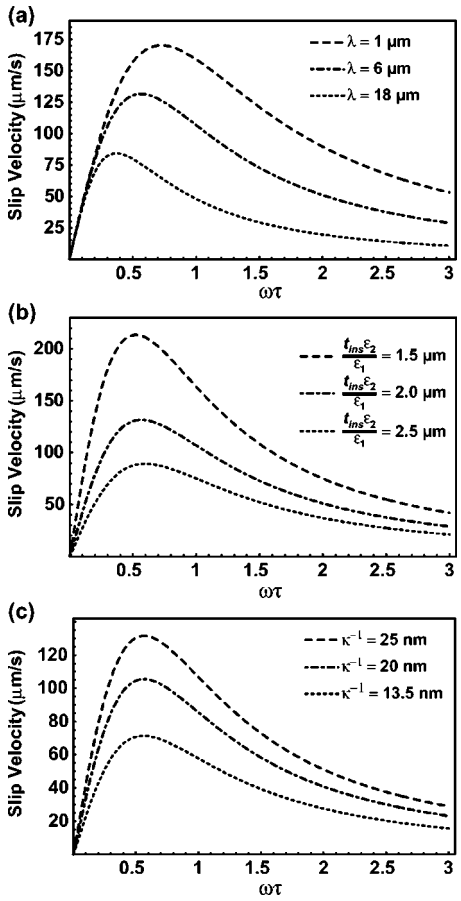

FIG. 6. Frequency dependence of electro-osmotic slip velocity as given by Eq. (50) using the following data: $\eta = 10^{-3}$ Ns/m^2, $\varepsilon_1 = 2.0\varepsilon_0$, $\varepsilon_2 = 80\varepsilon_0$, and $|\psi_a| = 250$ mV. (a) Slip velocity increases as the wavelength of the traveling wave decreases when $t_{ins}\varepsilon_2/\varepsilon_1 = 2$ μm and $\kappa^{-1} = 25$ μm. (b) Slip velocity increases as the factor $t_{ins}\varepsilon_2/\varepsilon_1$ decreases when $\lambda = 6$ μm and $\kappa^{-1} = 25$ μm. (c) Slip velocity increases as the Debye length increases when $\lambda = 6$ μm and $t_{ins}\varepsilon_2/\varepsilon_1 = 2$ μm.

C. Linearity conditions

In addition to the condition that $k_y \ll \kappa$ there are two other significant linearity conditions for these theoretical models: the surface potential condition (kT/ze) and the surface con-

ductivity condition (the Dukhin number). The surface potential can be divided into two components: the electrokinetic potential of the insulator surface ζ and the potential due to the ac excitation.

1. Electrokinetic potential

The electrokinetic potential is the equilibrium potential at the shear plane of the surface in the absence of a potential applied to the electrodes. For our experimental conditions, the electrokinetic potential of the HFP surface can be estimated from data describing Teflon surfaces from Kirby and Hasselbrink [56], that is, between −50 and −70 mV. This means that in our experiments the application of the traveling wave signal acts to perturb the equilibrium electric double layer while in our model the traveling wave is solely responsible for double layer formation. Nevertheless, the electrokinetic equations are not generally tractable analytically and the assumption of low potential makes an analytical solution possible and the treatment illustrates many of important factors that affect the phenomenon. Furthermore the time average of the product of the constant part of the double layer charge with the tangential field (alternating) is zero. The presence of this equilibrium electrokinetic potential probably acts to attenuate the electro-osmotic velocity.

2. Applied potential

In most colloid and interface science textbooks, it is stated that the Debye-Hückel approximation is limited to electrokinetic potentials less than kT/ze [41,43] or approximately 25 mV for univalent ions. Although counterintuitive, applying potentials of the order of 500 mV does not necessarily invalidate the linearity condition if the electrodes are insulated. The kT/ze limit is due to the linearization of the complete Poisson-Boltzmann equation. At higher potentials, the nonlinear complete solution to the Poisson-Boltzmann equation is valid.

At very low frequency, e.g., $\omega=0$, Eq. (41) agrees with the solution of the linearized Poisson-Boltzmann equation, that $\psi=\psi_b\exp(-\kappa x)$ which is a direct consequence of our simplification of the perturbation to the ion densities to sinusoidal form. In moving from Eq. (26) to Eq. (27), we state that the substitute variable h is negligible if $g<n^{\infty}$. In effect this condition is the origin of the kT/ze limit, if the perturbation to the concentration of positive and negative ions in the double layer is equal and opposite, linearization is valid. Only the component of the potential that is linearly related to the electric double layer charge is of significance, this is the potential drop across the double layer.

To understand how the applied potentials do not invalidate the linearity condition, it helps to recall how the potential is divided into two components in Eq. (38). Equation (41) can be split into these two components:

$$\varphi(x,y,t)=\mathrm{Re}\left\{\frac{\hat{\psi}_a\dfrac{\exp[i(\omega t-k_y y)-\kappa x\sqrt{1+i\omega\tau}]}{\kappa\sqrt{1+i\omega\tau}}}{\dfrac{1}{\kappa\sqrt{1+i\omega\tau}}+\dfrac{i\omega\tau}{k_y}+\dfrac{t_{ins}\varepsilon_2}{\varepsilon_1}(1+i\omega\tau)}\right\}\quad\text{and}\tag{51}$$

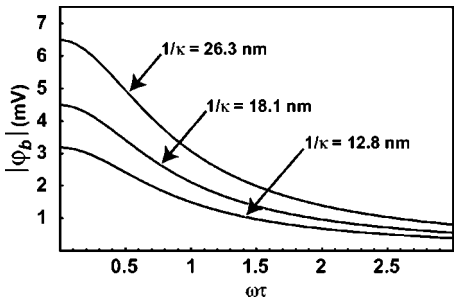

FIG. 7. Data generated using Eq. (51) showing the potential drop across the electric double layer due to the applied potential for the Debye lengths of the three solutions used in our experiments using: $\eta=10^{-3}$ Ns/m^2, $\varepsilon_1=2.0\varepsilon_0$, $\varepsilon_2=80\varepsilon_0$, $\lambda=6$ μm, $|\psi_a|=500$ mV.

$$\phi(x,y,t)=\mathrm{Re}\left\{\frac{\hat{\psi}_a\dfrac{i\omega\tau\exp[i(\omega t-k_y y)-k_y x]}{k_y}}{\dfrac{1}{\kappa\sqrt{1+i\omega\tau}}+\dfrac{i\omega\tau}{k_y}+\dfrac{t_{ins}\varepsilon_2}{\varepsilon_1}(1+i\omega\tau)}\right\}.\tag{52}$$

The first component φ satisfies Poisson's equation and can be related to the charge density in the double layer and its amplitude reduces with increasing frequency. The second component ϕ satisfies Laplace's equation and its amplitude increases from zero at low frequencies to a value much greater than φ at even relatively low frequencies. If $k_y\ll\kappa$, ϕ can be considered constant across the double layer so that $|\varphi_b|$ corresponds to the potential dropped across the double layer. Figure 7 shows how $|\varphi_b|$ decreases with increasing frequency and is always less than 10 mV for our experimental conditions.

3. Surface conductivity

The electrical conductivity is directly related to the ionic concentration. The formation of the double layer can result in a local perturbation to the ionic concentration so that the conductivity in the region of the electric double layer differs from that of the bulk fluid. This deviation is referred to as surface conductivity [43,57,58]. Surface conductivity is inversely proportional to a characteristic length of the system, for example, the radius of a capillary in capillary electro-osmosis. For our electrode structure, the inverse of k_y serves as the characteristic length.

The Dukhin number Du is the ratio of surface conductivity to bulk conductivity and is given by

$$Du\approx\frac{k_y}{\kappa}\left[\cosh\left(\frac{Vze}{2kT}\right)-1\right],\tag{53}$$

where V is the potential drop across the double layer. Surface conductivity effects will invalidate both of the models described above if the Dukhin number is not much less than one. Bazant *et al.* show how exceeding a limit similar to Du leads to strongly nonlinear behavior, that is, to bulk concentration gradients and, at very high voltages, transient space charge [59].

The Dukhin number is much less than 1 for our experimental conditions. For surface conductivity to influence ac

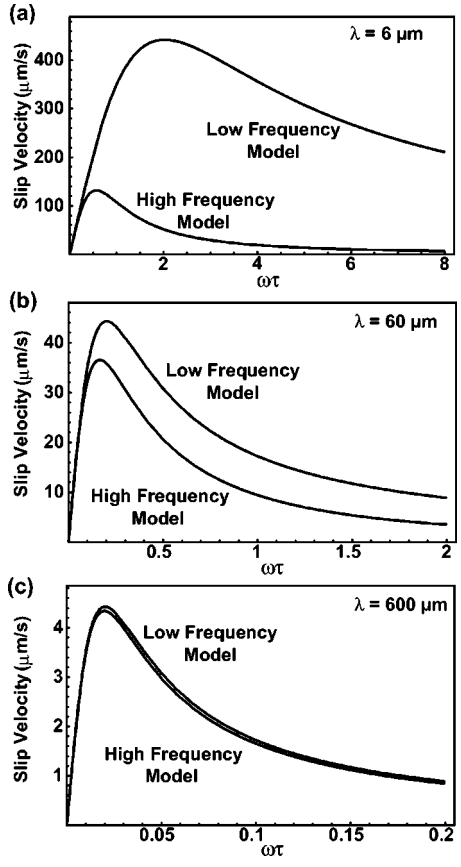

FIG. 8. Frequency dependence of the two models for the electro-osmotic slip velocity as given by Eqs. (9) and (50) using the following data: $\eta=10^{-3}$ Ns/m^2, $\varepsilon_1=2.0\varepsilon_0$, $\varepsilon_2=80\varepsilon_0$, $|\psi_a|=250$ mV, $t_{ins}\varepsilon_2/\varepsilon_1=2\mu$m, and $\kappa^{-1}=25$ nm. (a), (b), and (c) show how the two models converge as the wavelength increases from 6 to 60 μm and 600 μm, respectively.

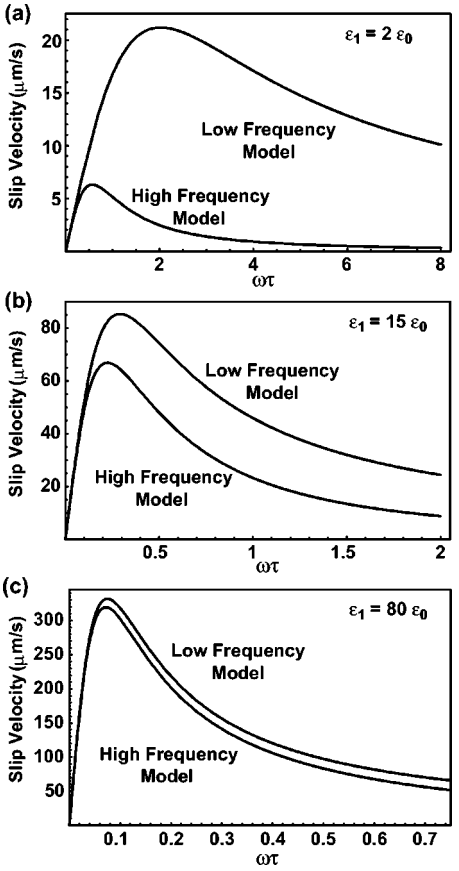

FIG. 9. Frequency dependence of the two models for the electro-osmotic slip velocity as given by Eqs. (9) and (50) using the following data: $\eta=10^{-3}$ Ns/m^2, $\lambda=6$ μm, $\varepsilon_2=80\varepsilon_0$, $|\psi_a|=250$ mV, $t_{ins}\varepsilon_2/\varepsilon_1=2\mu$m, and $\kappa^{-1}=25$ nm. (a), (b), and (c) show how the two models converge as ε_1 increases from $2.0\varepsilon_0$ to $15\varepsilon_0$ and $80\varepsilon_0$, respectively.

electro-osmotic flow, one might expect the frequency of maximum slip velocity to be greater than that predicted by the models, in much the same way as surface conductivity affects dielectrophoresis [60].

D. Discussion

Equations (9) and (50) have a similar form and exhibit primary dependence on the term $\varepsilon_2|\hat{\psi}_a|^2\omega\tau/(2\eta\kappa)$. The difference between the two expressions is that Eq. (50) contains the term $1+i\omega\tau$ three times. Two of these cases account for the relaxation of the double layer and the third is significant because the capacitance of the insulating layer does not relax at high frequencies.

Figure 8 shows how the two models converge when the wavelength of the structure is long. Equation (5) shows that ω_c is inversely proportional to wavelength, so that longer wavelengths lead to ω_c values that are much less than the double layer relaxation frequency. Figure 9 shows how the two models converge as the dielectric constant of the insulation layer increases, this is equivalent to increasing the capacitance of the insulating layer so that the capacitance of the double layer predominates, so that $\delta<1$. It is also possible to decrease the thickness of the insulating layer to similar effect. The two models converge when $\omega_c\tau\ll1$, where ω_c is given by Eq. (5), because the extra terms included in Eq. (50) disappear. If the condition $\omega_c\tau\ll1$ is not fulfilled, the first model becomes invalid and it is more correct to use the second model. The relaxation frequency of the second model never exceeds the double layer relaxation frequency.

Equations (9) and (50) predict fluid flow in the same direction as was observed experimentally. This rules out the possibility that the fluid flow is caused by traveling-wave induced electroconvection [34–37]. Traveling-wave dielectrophoresis [40] would cause bead motion in the same direction but this possibility may be discounted because a dielectrophoretic relaxation was observed for frequencies of the order of 5 MHz for the prepared latex bead dispersions, that is, for frequencies lower than 5 MHz beads were attracted to the electrodes and at higher frequencies they were repelled from the electrodes. This is consistent with the work of Hughes *et al.* [60] who observed a dielectrophoretic relaxation at similar frequencies for carboxylate latex beads in aqueous electrolytes of the same conductivity range. Traveling-wave dielectrophoresis takes place at frequencies in the range of a dielectrophoretic relaxation [40].

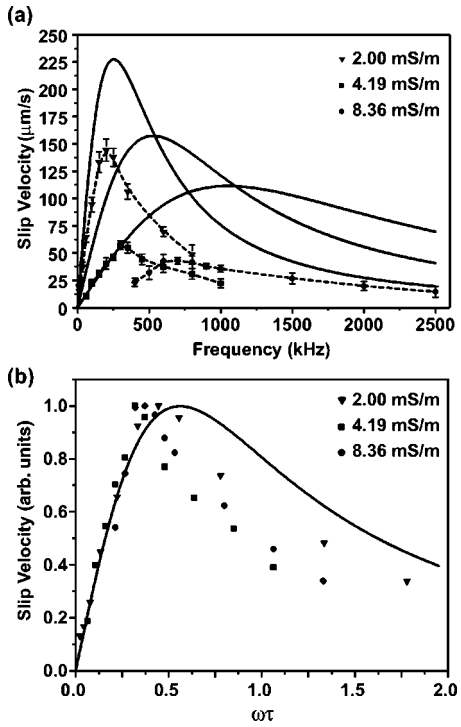

FIG. 10. (a) Experimentally measured values of the velocity of the fluorescent latex beads plotted against frequency at an applied potential of 450 mV at three different medium conductivities: 2.0 mS/m (▼), 4.19 mS/m (■), and 8.36 mS/m (•), that is, Debye lengths of 26.3, 18.1, and 12.8 nm, respectively. The dotted line is fitted to the experimental data. The behavior predicted Eq. (50) is shown by the continuous lines. The square wave of 450-mV amplitude is represented by the first harmonic of the Fourier series. (b) The same data normalized to the peak value measured and plotted against the radial frequency multiplied by the double layer relaxation time. The line fitted to the experimental data points is from Eq. (50).

We only compare the experimental results with the second model, as ω_c is greater than the double layer relaxation frequency. This is because of (i) the small width of electron-beam-microfabricated electrodes, and (ii) the factor δ is much greater than one because the thickness of the insulating layer is of the same order of the Debye length while its dielectric constant is much lower than that of water. Figure 10(a) shows the experimental data for the observed velocity of the fluorescent latex beads for each of the three electrolytic solutions for an applied potential of 450 mV amplitude as a function of frequency. These data were previously presented in Fig. 2. This shows how for the identical applied potential and increasing electrolyte conductivity the velocity decreases and the frequency of peak velocity shifts to higher frequencies.

There are some significant differences between theory and experiment. The experimentally observed velocity is significantly less than the predicted value. The decrease of velocity with increasing electrolyte conductivity is not as predicted by Eq. (50) although it does decrease with increasing conductivity. We concur with the observation of Brown *et al.* [24] that the observed velocity is a function of the life of the electrode structure. González *et al.* [22] also noted that the velocity predicted by theory was higher than that measured experimentally. The deviations observed in our experiments are probably due to the equilibrium electrokinetic potential of the surface being not only nonzero but greater than kT/ze so that the linearization is not fulfilled. In Sec. IV C, we note how the electrokinetic potential in the absence of an applied potential dominates the formation of the double layer at all frequencies and that the applied potential merely acts to perturb the electrokinetic potential. It is likely that the dependence of velocity on conductivity is linked to the dependence of the electrokinetic potential on conductivity in a way that is not taken into account by Eq. (50).

Figure 10(b) makes use of the same data as Fig. 10(a) but the velocity is normalized to the peak value for each curve and the angular frequency ω is normalized by multiplication with the double layer relaxation time τ. The data are fitted to Eq. (50), the normalization of both frequency and velocity leads to a curve that is largely independent of medium conductivity, if $k_y \ll \kappa$. It is clear that while the theory does not perfectly model our results that the form of the predicted curve is similar to the experimental results and that the frequency of the peak velocity is lower than but of the same order as that predicted. It is also clear that while there is some scatter in the frequency of peak velocity and that the conductivity range examined is not very large that the variation of the frequency of peak velocity with electrolyte conductivity is roughly that predicted by Eq. (50).

Figure 2 shows how the frequency of peak velocity is independent of applied potential; at least for the low applied potentials used in this study and presumed by our model. Equation (50) relates the slip velocity to the Debye length and consequently to the inverse of the square root of conductivity. Figure 3 shows that the experimentally observed velocity confirms the prediction of Eq. (50) that the electroosmotic slip velocity is proportional to the square of the applied potential. That we have observed this proportionality can be used to support the validity of the model on the basis of the low potentials applied to the electrodes.

It must be noted that the experimental setup implemented is more complicated than the theoretical model used to describe the system but that it is a suitable prototype to demonstrate the principle of traveling-wave induced electroosmotic flow. First, we chose to conduct our experiments using a spiral electrode structure and then chose to simulate a linear electrode structure. This point is mitigated by the fact that all of the relevant dimensions, for example of the radius of curvature of the spiral structure are much larger than the Debye length, so that on the scale of the Debye length the radius of curvature of the spiral appears to be flat. Second, we presume an idealized traveling wave that is a pure sinusoid both in the plane of the electrodes and in the plane of the interface between the insulating layer and the fluid. In practice, the application of a four-phase square wave signal to an electrode structure leads to a distorted traveling wave that is neither spatially or temporally identical to the ideal traveling wave. Also, the electrodes are not infinitely thin, they are 80 nm thick, indeed they are thicker than both the insulating layer (50 nm) and the Debye length ($<$27 nm). This thickness could act to attenuate the flow by acting as a surface roughness, surface roughness acts to re-

duce the velocity of electrokinetic flows [61]. Furthermore, field enhancement occurs at the edge of an electrode that may lead to further distortion of the traveling-wave signal. Third, we trace the movement of latex beads in order to ascertain the fluid velocity, the electric field is distorted by the presence of the beads and the beads themselves may be affected by dielectrophoresis [40]. At higher applied potentials the beads are attracted towards the electrodes by positive dielectrophoresis and their transport by fluid motion ceases. Finally, we simplify the nature of the dielectric interface by neglecting the influence of the Stern layer and the zeta potential of the surface [56]. In this case, the Stern layer capacitance is in series with the capacitance of the insulating layer and should be negligible but we estimate that the electrokinetic potential of the Teflon-like surface is around twice kT/ze. The theoretical approach presented in this paper is simplified to an extent but captures the qualitative trends of the experimental results and is sufficient to explain the core concepts at the heart of the phenomenon.

Equation (50) proves useful in describing the important factors on which this form of electro-osmosis depends and in demonstrating that fluid flow of this kind can take place for low applied potentials and the experimental results show that many of the most important factors, such as, the frequency profile of slip velocity, the frequency of maximum velocity and the proportionality of the velocity to the square of the applied potential agree well with Eq. (50). It offers insight into how electro-osmotic flow can be optimized.

V. CONCLUDING REMARKS

In this paper, we have shown that electro-osmotic streaming of electrolytes with conductivity in the range of $2-8$ mS/m can be driven by applying traveling-wave signals. Two theoretical models were derived which describe such electro-osmotic flow as a function of the amplitude of the applied electrical potential, the signal frequency, and the material properties of the system. The direction of streaming, the relationship of applied potential to velocity, and the frequency of maximum velocity with varying medium conductivity frequency agree well with that predicted by Eq. (50).

In common with other forms of electro-osmotic flow, this method has a pronounced advantage over pressure-driven flows because it continues to pump effectively as the dimension of the channel is reduced. For pressure-driven flows, the pressure gradient must increase as the square of the inverse of channel size to maintain a given fluid speed. In addition, pressure-driven flows often require external equipment, which is a major disadvantage for lab-on-chip applications. The observed streaming is caused by a noncontact method that requires no moving parts and can be controlled externally.

In common with the previously reported types of ac electro-osmotic flow, the performance of the system improves with miniaturization and the extension of the method to electrolytes of higher concentrations should be possible. Also the use of alternating signals and low potentials means that the method does not suffer from negative effects, such as bubble formation or excessive heating that afflict conventional dc electro-osmosis. In comparison with previously reported forms of ac electro-osmotic flow, translational flow was achieved using traveling waves where changing the direction of travel of the traveling wave reverses the direction of streaming, thus allowing flexible external control. The use of asymmetry suggested by Ajdari [23] does result in electrode structures that are more practical to fabricate and use but we believe that the principle of transferring the asymmetry from the geometry of the electrodes to the application of electrical signals can overcome this problem and that the phase shift between the signals applied to the electrodes is a form of asymmetry.

The amplitude of the applied signals is considerably lower than that required by conventional direct current electro-osmosis and because of the very thin electrodes used slightly lower than the previously reported types of ac electro-osmosis. This point is significant because the low amplitude required by this method is highly compatible for use with commercial batteries, considerably simplifying the integration of the method into low-cost lab-on-a-chip applications.

ACKNOWLEDGMENTS

We extend special thanks to Helmut Schift and Christian David, and thank Dieter Bächle, Bianca Haas, Brigitte Ketterer, and Harun Solak of PSI for help with microfabrication. We thank Guy Birrer for electronic circuit design and Olivier J. F. Martin for interesting discussions. Polyproject NANO II of the ETHZ supported this work.

[1] S. Shoji and M. Esashi, J. Micromech. Microeng. **4**, 157 (1994).
[2] S. Devasenathipathy, J. G. Santiago, and K. Takehara, Anal. Chem. **74**, 3704 (2002).
[3] A. E. Herr *et al.*, Anal. Chem. **72**, 1053 (2000).
[4] J. G. Santiago, Anal. Chem. **73**, 2353 (2001).
[5] R. B. M. Schasfoort, S. Schlautmann, L. Hendrikse, and A. van den Berg, Science **286**, 942 (1999).
[6] A. Brask, G. Goranovic, and H. Bruus, Sens. Actuators B **92**, 127 (2003).
[7] Y. Takamura *et al.*, Electrophoresis **24**, 185 (2003).
[8] A. Ajdari, Phys. Rev. Lett. **75**, 755 (1995).
[9] A. Ajdari, Phys. Rev. E **53**, 4996 (1996).
[10] A. Ajdari, Phys. Rev. E **65**, 016301 (2002).
[11] D. Long, H. A. Stone, and A. Ajdari, J. Colloid Interface Sci. **212**, 338 (1999).
[12] F. Nadal *et al.*, Eur. Phys. J. E **9**, 387 (2002).
[13] A. D. Stroock *et al.*, Phys. Rev. Lett. **84**, 3314 (2000).
[14] A. D. Stroock *et al.*, Anal. Chem. **74**, 5306 (2002).
[15] A. D. Stroock *et al.*, Science **295**, 647 (2002).
[16] M. Trau, D. A. Saville, and I. A. Aksay, Langmuir **13**, 6375 (1997).

[17] S. R. Yeh, M. Seul, and B. I. Shraiman, Nature (London) **386**, 57 (1997).
[18] A. Ramos *et al.*, J. Electrost. **163**, 137 (1999).
[19] A. Ramos *et al.*, J. Colloid Interface Sci. **217**, 420 (1999).
[20] N. G. Green *et al.*, Phys. Rev. E **61**, 4011 (2000).
[21] N. G. Green *et al.*, Phys. Rev. E **66**, 026305 (2002).
[22] A. González *et al.*, Phys. Rev. E **61**, 4019 (2000).
[23] A. Ajdari, Phys. Rev. E **61**, R45 (2000).
[24] A. B. D. Brown, C. G. Smith, and A. R. Rennie, Phys. Rev. E **63**, 016305 (2001).
[25] A. Ramos *et al.*, Phys. Rev. E **67**, 056302 (2003).
[26] V. Studer, A. Pepin, Y. Chen *et al.*, Microelectron. Eng. **61-2**, 915 (2002).
[27] M. Mpholo, C. G. Smith, and A. B. D. Brown, Sens. Actuators B **92**, 262 (2003).
[28] R. M. Ehrlich and J. R. Melcher, Phys. Fluids **25**, 1785 (1982).
[29] J. W. Choi and Y. K. Kim, in *30th IAS Annual Meeting Conference Record* (IEEE, New York, 1995), pp. 1480–1484.
[30] A. P. Washabaugh, M. Zahn, and J. R. Melcher, IEEE Trans. Electr. Insul. **24**, 807 (1989).
[31] S. F. Bart *et al.*, Sens. Actuators, A **21**, 193 (1990).
[32] J. R. Melcher, Phys. Fluids **9**, 1548 (1966).
[33] J. R. Melcher and M. S. Firebaugh, Phys. Fluids **10**, 1178 (1967).
[34] G. Fuhr *et al.*, J. Microelectromech. Syst. **1**, 141 (1992).
[35] G. Fuhr, T. Schnelle, and B. Wagner, J. Micromech. Microeng. **4**, 217 (1994).
[36] J. Gimsa, P. Eppmann, and B. Pruger, Biophys. J. **73**, 3309 (1997).
[37] T. Müller *et al.*, Electrophoresis **14**, 764 (1993).
[38] C. David and D. Hambach, Microelectron. Eng. **46**, 219 (1999).
[39] H. F. Knapp and A. Stemmer, Surf. Interface Anal. **27**, 324 (1999).
[40] T. B. Jones, *Electromechanics of Particles* (Cambridge University Press, New York, 1995).
[41] R. J. Hunter, *Foundations of Colloid Science* (Oxford University Press, Oxford, 2001).
[42] G. E. Karniadakis and A. Beskok, *Micro Flows: Fundamentals and Simulation* (Springer, New York, 2002), Chap. 8.
[43] J. Lyklema, *Fundamentals of Interface and Colloid Science: Volume II Solid-Liquid Interfaces* (Academic Press, London, 1995).
[44] M. v. Smoluchowski, Bull. Int. Acad. Sci. Cracovie **8**, 182–193 (1903).
[45] H. Isambert, A. Ajdari, J. L. Viovy, and J. Prost, Phys. Rev. E **56**, 5688 (1997).
[46] R. W. O'Brien, J. Colloid Interface Sci. **92**, 204 (1983).
[47] S. S. Dukhin and V. N. Shilov, *Dielectric Phenomena and the Double Layer in Disperse Systems and Polyelectrolytes* (Wiley, New York, 1974).
[48] E. M. Trukhan, Fiz. Tverd. Tela (S.-Peterburg) **4**, 3496 (1962) [Sov. Phys. Solid State **4**, 2560 (1963)].
[49] J. R. Melcher and G. I. Taylor, Annu. Rev. Fluid Mech. **1**, 111 (1969).
[50] J. L. Anderson, J. Colloid Interface Sci. **105**, 45 (1985).
[51] J. L. Anderson, W. K. Idol, Chem. Eng. Commun. **38**, 93 (1985).
[52] J. L. Anderson, Annu. Rev. Fluid Mech. **21**, 61 (1989).
[53] P. Debye and E. Hückel, Phys. Z. **24**, 185 (1923).
[54] P. Debye and E. Hückel, Phys. Z. **24**, 305 (1923).
[55] J. R. Melcher, *Continuum Electromechanics* (MIT Press, Cambridge, MA, 1981), Sec. 4.5.
[56] B. J. Kirby and E. F. Hasselbrink, Electrophoresis **25**, 203 (2004).
[57] S. S. Dukhin and B. V. Derjaguin, in *Surface and Colloid Science*, edited by E. Matijevic (Wiley, New York, 1974), Vol. 7.
[58] J. J. Bikerman, Z. Phys. Chem. Abt. A **163**, 378 (1933).
[59] M. Z. Bazant, K. Thornton, and A. Ajdari, Phys. Rev. E **70**, 021506 (2004).
[60] M. P. Hughes, H. Morgan, and M. F. Flynn, J. Colloid Interface Sci. **220**, 454 (1999).
[61] Y. Hu, C. Werner, and D. Li, Anal. Chem. **75**, 5747 (2003).